Cellular & Molecular Immunology (2016) 13, 191–205

www.nature.com/cmi

RESEARCH ARTICLE

Immunomodulatory properties of silver nanoparticles contribute to anticancer strategy for murine fibrosarcoma

Biswajit Chakraborty[1], Ramkrishna Pal[1], Mohammed Ali[2], Leichombam Mohindro Singh[1], Dewan Shahidur Rahman[2], Sujit Kumar Ghosh[2] and Mahuya Sengupta[1]

The use of nanotechnology in nanoparticle-based cancer therapeutics is gaining impetus due to the unique biophysical properties of nanoparticles at the quantum level. Silver nanoparticles (AgNPs) have been reported as one type of potent therapeutic nanoparticles. The present study is aimed to determine the effect of AgNPs in arresting the growth of a murine fibrosarcoma by a reductive mechanism. Initially, a bioavailability study showed that mouse serum albumin (MSA)-coated AgNPs have enhanced uptake; therefore, toxicity studies of AgNP-MSA at 10 different doses (1–10 mg/kg b.w.) were performed in LACA mice by measuring the complete blood count, lipid profile and histological parameters. The complete blood count, lipid profile and histological parameter results showed that the doses from 2 to 8 mg (IC_{50}: 6.15 mg/kg b.w.) sequentially increased the count of leukocytes, lymphocytes and granulocytes, whereas the 9- and 10-mg doses showed conclusive toxicity. In an antitumor study, the incidence and size of fibrosarcoma were reduced or delayed when murine fibrosarcoma groups were treated by AgNP-MSA. Transmission electron micrographs showed that considerable uptake of AgNP-MSA by the sentinel immune cells associated with tumor tissue and a morphologically buckled structure of the immune cells containing AgNP-MSA. Because the toxicity studies revealed a relationship between AgNPs and immune function, the protumorigenic cytokines TNF-α, IL-6 and IL-1β were also assayed in AgNP-MSA-treated and non-treated fibrosarcoma groups, and these cytokines were found to be downregulated after treatment with AgNP-MSA.
Cellular & Molecular Immunology (2016) **13**, 191–205; doi:10.1038/cmi.2015.05; published online 4 May 2015

Keywords: AgNP-MSA; fibrosarcoma; IL-1β; IL-6; immunomodulation; nanoparticles; TNF-α

INTRODUCTION

The use of nanoparticles to fight the dreaded disease of cancer has recently created new possibilities in the field of cancer therapeutics and thus demands further research on the overall effect of nanoparticles, especially *in vivo*. The immune system has the ability to fight against tumors as well as other diseases because of the multiple immune checkpoints within cells that regulate or dictate tumor immune surveillance inside an organism; many of these checkpoints are bypassed in tumor microenvironments. Thus, targeting these altered immune checkpoints by adoptive T-cell therapy, the use of chimeric antigen receptors or the induction of multiple inflammatory pathways within the tumor microenvironment are the foremost targets in the field of cancer immunotherapy.[1]

Nanoparticles are associated with immune systems and either act as immunostimulants or immunosuppressors. Nanoparticles are often first taken up by the phagocytic cells of the immune system (e.g., macrophages and dendritic cells); through undesirable interactions between nanoparticles and the immune system, nanoparticles may promote either inflammatory or anti-inflammatory responses. Immune cells may consider nanoparticles to be foreign entities, thus resulting in an inadvertent multilevel immune response against the nanoparticles (e.g., allergic response); this response may ultimately lead to toxicity inside the biological system. The physical characteristics of nanoparticles, such as size, surface charge, hydrophobicity/hydrophilicity and the steric effects of their coatings, can dictate the compatibility between the nanoparticles and the immune system.[2]

Silver nanoparticles (AgNPs) are among the most commercialized nanoparticles because of their unique optical, catalytic and disinfectant properties. Currently, AgNPs are being used for many different applications,[3–5] ranging from wound dressing and the coatings of surgical instruments and prostheses[6,7]

[1]Immunobiology Laboratory, Department of Biotechnology, Assam University, Silchar, India and [2]Department of Chemistry, Assam University, Silchar, India
Correspondence: Dr M Sengupta, Immunobiology Laboratory, Department of Biotechnology, Assam University, Silchar 788011, India.
E-mail: senguptamahuya35@gmail.com
Received: 16 September 2014; Revised: 8 January 2015; Accepted: 8 January 2015

to the use in food container systems or as the coating material for certain household devices, such as washing machines. AgNPs are being incorporated into textiles and are also added to cosmetics.[8,9]

Recent research throughout the world has indicated that AgNPs also induce immunologic response inside biological hosts, including immune cells.[10] Nanocrystalline silver was observed to induce the apoptosis of inflammatory cells through suppression of TNF-α and IL-12.[11] It has been reported that AgNPs interact with the HIV-1 virus via gp120 glycoprotein knobs. In fresh water fishes, AgNPs are known to be associated with an inflammatory response.[12] AgNPs have also been shown to inhibit molecules related to the cholinergic system and consequently impair the immune system differentiation in zebrafish.[13] AgNPs behave as allergens in mice, as reported in a recent proteome-based study.[14] The intravenous administration of AgNPs also showed immunotoxicity in murine models.[15] Respiratory tract immune toxicity has also been associated with AgNPs.[16] AgNP treatment of peripheral blood mononuclear cells and human mesenchymal stem cells showed inhibition of the production of cytokines, such as IFN-γ, IL-6, IL-8, IL-11, TNF-α and more weakly, IL-5.[17] In a recent *in vitro* study, AgNP exposure showed an induction of expression of IL-8 and stress genes in macrophages.[18] In toxicity studies of AgNPs, a dose of more than 10 mg/kg b.w. in rats showed liver toxicity.[19] Moreover, in *in vitro* and *in vivo* studies conducted by Sriram *et al.*,[20] it was shown that AgNPs have antitumor properties against Dalton's lymphoma ascites tumor model. Thus, recent findings suggest that there is a relationship between AgNPs and the immune system, however, there are almost no reports on the AgNP immunomodulation of tumor-bearing mice. Although there are several reports on the toxicity of AgNPs,[21–25] there is a paucity of toxicity studies on the AgNP dose-response in mice. Hence, the present investigation was designed to determine the effects of AgNPs at different doses in mice and to study their effects on murine fibrosarcoma. Chemically induced tumors in inbred mice, particularly sarcomas induced by 3-methylcholanthrene (3-MCA), have been a favorite model of tumor immunologists since the discovery of their antigenic properties.[26,27] The discovery of immunomodulating cytokines has strongly established the immunological influences of tumor induction in chemically induced fibrosarcoma.[28] For this purpose, a modified murine two-stage carcinogenesis model was adopted in which a single subcutaneous administration of the carcinogen 3-MCA (0.5 mg/mouse) was followed by multiple applications of the tumor promoter phorbol myristate 13-acetate (PMA) administered subcutaneously (s.c.).[29]

MATERIALS AND METHODS

Synthesis of mouse serum albumin (MSA)-stabilized AgNPs

Mouse serum albumin (Sigma-Aldrich, USA) or MSA-stabilized AgNPs were prepared by a ligand exchange reaction on citrate-stabilized AgNPs following the method reported by Duncan Graham and co-workers.[30] All glassware was cleaned with aqua regia and thoroughly rinsed with distilled water. Ag-citrate nanoparticles were prepared according to the Lee–Meisel procedure.[30] A clean three-necked round bottom flask was filled with 500 ml of Milli-Q water. The solution was heated to 45 °C using a Bunsen burner under continuous stirring with a glass stirrer. Then, silver nitrate (90 mg dissolved in 10 ml of Milli-Q water) was added. The solution was heated further to 98 °C. Trisodium citrate (100 mg in 10 ml Milli-Q water) was added, and the solution was kept at 98 °C for 90 min; afterwards, the solution was allowed to cool to room temperature. Citrate-stabilized AgNPs were further functionalized with MSA in a ligand exchange reaction. In a typical method, a methanolic solution of MSA (2.5 μl, 40 mM) was added to a 10 ml nanoparticle dispersion, and the mixture was stirred for 3 h, while protected from light. The excess ligand was removed by centrifugation and redispersed in Milli-Q water. These nanoparticles were characterized by UV-Vis spectrometry (Shimadzu UV-1601 digital spectrophotometer (Shimadzu, Japan)), transmission electron microscopy (JOL, JSM-2100; JEOL, Japan) and Fourier transform infrared spectroscopy (FTIR) analysis. The MSA loading on the nanoparticles was determined from the entrapment efficiency (EE), which was spectrophotometrically estimated at 595 nm using the following equation:[31]

$$\mathbf{EE} = (\mathbf{Total\ initial\ amount\ of\ MSA\ added} - \mathbf{Free\ amountof\ MSA\ insupernatant}) \times (\mathbf{Totalinitial\ amount\ of\ MSA\ added})^{-1} \times \mathbf{100}$$

Animals

The LACA male albino mice were purchased from The Pasteur Institute, Shillong, India (license no.: 34/DR/1966). The 6- to 8-week old male mice having body weights of 20±2.0 g were used for all the experiments. All treatments were performed in accordance with the guidelines of the Institutional Ethics Committee. All animals were housed in polycarbonate cages at 22±2 °C temperature, 85% relative humidity and a 12-h light–darkness cycle with standard food and water available *ad libitum*.

Bio-distribution of AgNPs

Samples of 500 mg each of the collected liver, kidney and spleen tissues from normal mice groups treated with different concentration of AgNPs and AgNP-MSA were weighed and dissolved in 4 ml of aqua regia. These were then heated at 80 °C for 10 min to dissolve the tissue. The same procedure was also used for tumor tissue treated with both AgNP and AgNP-MSA at the selected antitumor dose of 4 mg/kg b.w. All dissolved tissues were then examined for the uptake of AgNPs by inductively coupled plasma atomic emission spectroscopy (ICP–AES).

Experimental design for toxicity study

For the toxicity study, a total of 55 mice were divided into 11 groups, with 5 mice in each group. The first group was kept as a control, and the other 10 groups were administered (subcutaneously on alternate days) varying doses (1–10 mg/kg b.w.) of with AgNP-MSA separately. Weekly analyses of the complete

blood count and lipid profile were performed for all the groups. After 4 weeks of treatment, all of the mice were then euthanized following analysis of the complete blood count, lipid profile and histological parameters.

Hematological analysis

Heparinized blood was collected in EDTA-coated vials by intra cardiac puncture after anesthetization with chloroform. We examined the erythrocyte counts (RBC), mean corpuscular volume, RBC distribution width (RDW%), RDWa, hematocrit, platelet count, mean platelet volume, platelet distribution width, procalcitonin, large platelet concentration ratio, leukocyte count (white blood cell (WBC)), hemoglobin, mean corpuscular hemoglobin, mean corpuscular hemoglobin content, lymphocyte count, granulocyte count and mid cell count from the whole blood with the help of an automated hematological analyzer (Piramal photometer 5010 V5+; Piramal Enterprise Limited, India).

Serum analysis

To analyze the effect of AgNPs on liver and renal function, the serum levels of the following were measured in the different experimental groups and compared with those of the control mice: alanine transferase (ALT), aspartate transferase (AST), alkaline phosphatase, creatinine, triglycerides, total cholesterol, high-density lipoprotein, low-density lipoprotein and very low-density lipoprotein. Moreover, for further antitumor experimental studies, the IC50 of AgNPs was determined from the reduction in the serum ALT level.

Histological analysis

To determine the effect of the administration of different AgNP concentrations on various organs, such as the liver, kidney and spleen, histological analysis was performed. After 4 weeks of treatment and following the euthanasia of the treated mice, the liver, kidney and spleen tissues were fixed with 4% paraformaldehyde. The fixed tissue samples were then transferred to 30% sucrose for 24 h prior to cryo-sectioning. After the tissues were sectioned to a size of 10 μm, the sections were stained with hematoxylin and eosin. The AgNP toxicity was determined by observing the histological sections under a light microscope for any deviation from the control slides.

***In vivo* antitumor experimental design**

For the antitumor experiment, two groups of 20 male mice each were used. To develop the fibrosarcoma model, both groups were treated with a single dose (0.5 mg/mice) of MCA (s.c.) and PMA (s.c. 4.26 nM on alternate days) for 40 weeks.[29,32] Of these, one group was also given AgNP-MSA at a dose of 4 mg/kg b.w. (s.c. on alternate days) from the second week until the fortieth week of treatment. Parameters, such as the incidence of tumor, change in body weight, variation in tumor size, and serum TNF-α, IL-6 and IL-1β levels, were then measured for these two groups. To analyze the effect of AgNPs on the serum cytokine levels of the tumor group, TNF-α, IL-6 and IL-1β were measured using ELISA kits from BD Biosciences (BD OptEIA, USA). The manufacturer's protocol was employed in the measurement, and the enzyme-substrate reaction was terminated by the addition of sulfuric acid solution, after which any color change was observed spectrophotometrically in an ELISA reader (Bio-Rad, Germany) at 595 nm.

The nitroblue tetrazolium (NBT) assay

The NBT assay was performed to obtain a quantitative estimation of the superoxide anion (O^{2-}) level in various tissues (liver, spleen, kidney and tumor). Membrane permeable, water-soluble NBT is used as an electron acceptor, and upon reduction by superoxide anions, NBT changes from a yellow solute to a blue formazan precipitate. Briefly, HBSS containing 0.1% NBT was added to the sample and kept at 370 °C for 2 h with occasional shaking. Then, the sample was washed with 70% methanol 3 times and dried at 600 °C for 15 min; 2 M potassium hydroxide, 8–10 μl of Triton X-100, and 500 μl of dimethylsulfoxide were added, and the mixture was allowed to rest for 10 min. The formazan was then solubilized in dimethylsulfoxide and potassium hydroxide, and the optical density of the solubilized formazan was subsequently measured spectrophotometrically at 620 nm. The concentration of NBT was calculated from the OD at 620 nm, and the extent of ROS in the sample was determined.[33]

Nitric oxide release assay (NO)

The nitric oxide release was quantitatively measured in different tissues (liver, spleen, kidney and tumor) using Griess reagent. Briefly, the tissue was converted to a single cell suspension, and then Griess reagent was added to 10^6 cells; the mixture was allowed to rest for 10 min. Then, to measure the released nitric oxide, the OD was determined using a spectrophotometer at 550 nm, and the OD was compared with a standard curve for sodium nitrate.[34]

Immunocytochemistry

Tumor tissues from treated and non-treated mice were removed and converted to a single cell suspension (SCS) using 0.5% trypsin dissolved in PBS. IL-1β tagged with phycoerythrin, which is fluorescent, was added to 10^6 cells according to the manufacturer's protocol (R&D Systems, USA). The tagged cells were observed under a fluorescence dark field microscope (Nikon TS 100 ECLIPSE, Japan).

Transmission electron micrograph analysis of fibrosarcoma tissue treated with AgNP-MSA

Transmission electron micrographs were obtained for both tumor tissue and AgNP-MSA-treated tumor tissue. The primary fixation of tissues for transmission electron microscopy was performed using Karnovsky fixative, and further fixations, including sample processing, were conducted at SAIF, NEHU, Shillong, India, where photographs were taken.

Statistical analysis

The obtained raw scores were plotted as a function of number of weeks of the test, and then statistical analyses, such as

Student's *t*-test, the Mann–Whitney *U*-test and ANOVA, were performed. The data are presented as the mean±standard error of mean (s.e.m.) for 20 mice/group with the significance level set at $P<0.05$.

RESULTS

Characterization of AgNP-MSA

The prepared AgNPs were characterized before being used as a potential antitumor agent. The surface plasmon band at 400 nm in the UV-Vis spectra (Figure 1a) of the AgNPs indicates that the AgNPs were successfully transformed into the nanometer regime. The morphology and size of the MSA-stabilized AgNPs were determined using transmission electron microscopy (TEM). Figure 1b is the TEM image of the prepared AgNPs, which clearly shows that the average size of the particles was approximately 10 nm and depicts that the AgNPs are relatively uniform in diameter and spherically shaped. As previously mentioned, the AgNP solution after ligand exchange (with MSA) was washed several times by ultra-centrifugation and redispersion to remove citrate and excess MSA. Figure 1c shows the FTIR spectra of pure MSA and MSA-stabilized AgNPs, and Table 1 lists the comparative peak assignment. In the case of pure protein, the peaks at 3290 cm^{-1}, 1622 cm^{-1} and 1517 cm^{-1} are attributed to the stretching vibration of amide A (mainly –NH stretching), amide I (−C=O stretching) and amide II (−CN stretching, −NH bending), respectively. In the case of MSA binding to AgNPs, negligible variations were observed in the characteristic peak of the amide I bands, but the characteristic peak of the amide II band shifted to a 40 cm^{-1} higher wavenumber, suggesting that there is a coordination interaction between the silver ions and MSA. Most notably, the characteristic peak of the amide A band shifts to the higher wavenumber of 3445 cm^{-1}. Such a large variation further suggests that coordination has formed between AgNPs and the amine groups of MSA, which plays an important role in the formation of MSA-stabilized AgNPs. Therefore, the FTIR spectroscopy result proves that MSA ligands are conjugated to the AgNPs. The EE of MSA on the AgNP surface was found to be 95%±2%.

Bio-distribution of AgNPs

The *in vivo* bioavailability analysis of AgNPs and MSA-coated AgNPs in normal mice showed that AgNPs alone had very low bioavailability, whereas AgNP-MSA showed a detectable bioavailability. This finding implied that the functionalized AgNPs (AgNP-MSA) have greater compatibility for uptake in an *in vivo* condition (Table 2). Because AgNP-MSA showed enhanced bioavailability in experimental LACA mice, AgNP-MSA was selected for further studies.

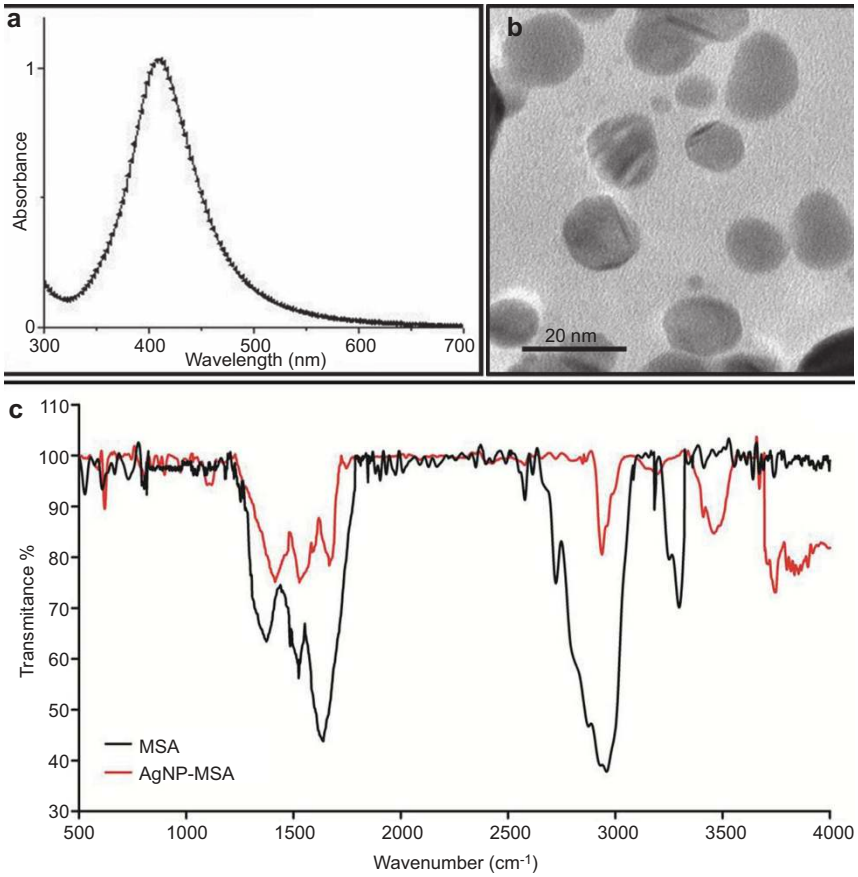

Figure 1 (**a**) UV-Vis spectra of MSA-capped silver nanoparticles. (**b**) TEM image of MSA-capped AgNPs. (**c**) FTIR spectra of MSA and AgNP-MSA. AgNP, silver nanoparticle; FTIR, Fourier transform infrared spectroscopy; MSA, mouse serum albumin; TEM, transmission electron microscopy.

Table 1 The main IR absorption bands of pure MSA and MSA attached to AgNPs

Designation	*Pure MSA (cm^{-1})*	*MSA-Ag (cm^{-1})*	*Description*
Amide-A	3290	3445	N–H stretching
Amide-I	1622	1642	C=O stretching
Amide-II	1517	1527	CN stretching and N–H bending

Abbreviations: AgNP, silver nanoparticle; MSA, mouse serum albumin.

Toxicity studies

Effect of AgNPs on the blood and lipid profile of control mice. The results from the complete blood count and lipid profile of AgNP-MSA-treated and non-treated normal mice showed no significant difference up to 8 mg/kg b.w. (Supplementary Figure 1 and Supplementary Figure 2). However, the doses from 2 to 8 mg/kg b.w. showed an increase in the WBC, lymphocytes and granulocytes of normal mice (Fig 2; $P<0.005$). In contrast, the doses of 9 and 10 mg/kg b.w. showed conclusive toxic effects on the mice, as indicated by some of the blood parameters (Table 3; $P<0.001$) and the complete lipid profile (Table 4; $P<0.01$). Additionally, from the AgNP-MSA-induced reduction in the serum alkaline phosphatase levels, the IC50 was determined to be 6.15 mg/kg b.w. (data not shown).

Effect of AgNPs on tissue (liver, spleen and kidney) damage. The liver sections were found to have normal architecture in all treated groups except those treated at the 9 and 10 mg/kg b.w. doses. Necrotic spots of hepatocytes and hydrophobic degeneration around the central vein were observed at these doses. At these two doses, inflammatory cells were found in the bile ducts, and multifocal lesions were observed in the spleen. No abnormality was observed in the kidney (Figure 3).

Effect of AgNPs on incidence of murine fibrosarcoma

First, whether AgNP-MSA had any effect on the MCA-induced and PMA-promoted solid tumor incidence was examined. A significant delay of 9 weeks was found in the first tumor incidence in the nanoparticle-treated group compared to the tumor-bearing mice that were not treated with AgNP-MSA. There was also a significantly lower tumor incidence in the nanoparticle-treated group; 85% of the mice showed a tumor when treated with only MCA and PMA, but the AgNP-MSA-treated mice had an incidence of only 15% at the fortieth week. Moreover, we estimated the tumor growth pattern by estimating a logistic curve which was fitted on the basis of the incidence (percentage) data. The logistic curve was generated by the following logistic growth equation:

$$Y = L/\left(1 + ae^{-bt}\right)$$

where Y is the tumor incidence given as a percentage (%), and 'a' and 'b' are the statistical parameters to be estimated from the experimental data. Here, 'L' is a scale parameter that scales the logistic curve 'up' or 'down.' We select the value of 'L' for which the mean standard error is minimum; the maximum of this value has been fixed at 100 because the Y data are in percentages.

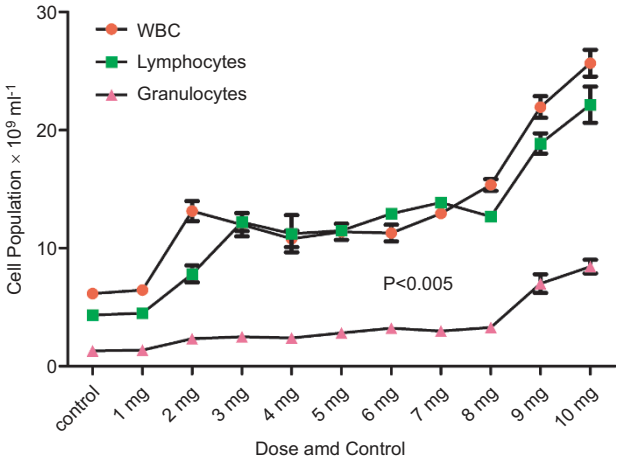

Figure 2 Effect of silver nanoparticles at various doses in normal LACA mice on the counts of immune cells, such as WBCs, lymphocytes and granulocytes. The results are expressed as the mean±s.e.m. ($P<0.005$). s.e.m., standard error mean; WBC, white blood cell.

Table 2 Biodistribution of AgNPs and AgNP-MSA in different tissues of treated LACA mice; the result was obtained from ICP–AES analysis

	Liver		*Spleen*		*Kidney*	
Dose (mg/kg b.w.)	*AgNPs*	*AgNP-MSA*	*AgNPs*	*AgNP-MSA*	*AgNPs*	*AgNP-MSA*
1	0.021±0.01 ppm	<0.01 ppm	<0.01 ppm	<0.01 ppm	<0.01 ppm	<0.01 ppm
2	0.467±0.23 ppm	<0.01 ppm	<0.01 ppm	<0.01 ppm	<0.01 ppm	<0.01 ppm
3	1.67±0.13 ppm	<0.01 ppm	0.027±0.003 ppm	<0.01 ppm	<0.01 ppm	<0.01 ppm
4	2.4745±0.16 ppm	<0.01 ppm	0.079±0.007 ppm	<0.01 ppm	<0.01 ppm	<0.01 ppm
5	2.7612±0.325 ppm	<0.01 ppm	0.0854±0.0025 ppm	<0.01 ppm	<0.01 ppm	<0.01 ppm
6	2.8732±0.47 ppm	<0.01 ppm	0.0873±0.0047 ppm	<0.01 ppm	<0.01 ppm	<0.01 ppm
7	2.8709±0.387 ppm	<0.01 ppm	0.09921±0.0037 ppm	<0.01 ppm	<0.01 ppm	<0.01 ppm
8	3.1557±0.7634 ppm	<0.01 ppm	0.117±0.0064 ppm	<0.01 ppm	<0.01 ppm	<0.01 ppm
9	3.113±0.023 ppm	<0.01 ppm	0.14±0.003 ppm	<0.01 ppm	<0.01 ppm	<0.01 ppm
10	3.421±0.12 ppm	0.03±0.053 ppm	0.131±0.017 ppm	0.03±0.053 ppm	0.0221±0.002 ppm	<0.01 ppm

Abbreviations: AgNP, silver nanoparticle; ICP–AES, inductively coupled plasma–atomic emission spectroscopy; MSA, mouse serum albumin.

Table 3 Blood toxicity profile of AgNP-MSA-treated LACA albino mice. The results are expressed as the mean±standard error mean ($P<0.001$)

Parameters	*Control*	*9 mg/kg b.w.*	*10 mg/kg b.w.*
RBC ($\times10^{12}$/l)	14.162±1.12	11.264±0.51	9.77±0.34**
MCV (fl)	46.954±0.85	46.9±1.31	48.32±1.33
RDW (%)	15.58±1.027	15.14±0.65	13.284±1.37
HCT (%)	51.52±1.75	46.286±1.28	48.274±1.29
PLT ($\times10^{9}$/l)	673±12.77	549.8±17.64	793.8±20.28
MPV (fl)	5.792±0.19	6.128±0.088	6.174±0.24
PDW (fl)	8.946±0.16	9.858±0.28	9.372±0.32
PCT (%)	0.452±0.02	0.312±0.05	0.484±0.02
HGB (g/dl)	16.74±0.67	10.77±1.21	10.32±0.71
MCH (pg)	16.98±0.44	12.44±0.53	15.348±0.33
MCHC (g/dl)	32.82±0.94	28.088±0.53	32.522±1.20

Abbreviations: AgNP, silver nanoparticle; HCT, hematocrit; HGB, hemoglobin; MCA, mean corpuscular volume; MCH, mean corpuscular hemoglobin; MCHC, mean corpuscular hemoglobin content; MPV, mean platelet volume; MSA, mouse serum albumin; PCT, procalcitonin; PDW, platelet distribution width; PLT, platelet count; RBC, red blood cell count; RDW, RBC distribution width.

Figure 4 implies that after the treatment with AgNPs, the logistic growth of the tumor incidence was significantly lower ($P<0.0001$). This drop in the growth rate of the tumor incidence can be attributed to the AgNP treatment, which was the sole treatment difference between the AgNP-treated group and the non-treated group.

Effect of AgNP-MSA on the body weight of mice with murine fibrosarcoma

There was a normal growth in body weight for the first few weeks, but after the twenty-fifth week, there was a significant loss of body weight (cachexia) in the tumor-bearing mice. However, observations of the physical activity and vitality of both the nanoparticle-treated and non-treated tumor-bearing mice indicated that the treated tumor-bearing mice were more active and healthy and had gained weight compared with the non-treated tumor group (Figure 5; $P<0.04$).

Table 4 Lipid toxicity profile of AgNP-MSA-treated LACA albino mice. The results are expressed as the mean±standard error mean ($P<0.01$)

Parameter	*Control*	*9 mg/kg b.w.*	*10 mg/kg b.w.*
AST (units/l)	50.57±1.05	107.20±4.42	133.80±3.10
ALT (units/l)	23.52±0.66	56.20±2.06	63.60±1.08
ALP (units/l)	89.70±0.85	73.40±1.60	55.20±1.43
Creatinine (mg/dl)	0.68±0.04	0.63±0.02	0.43±0.03
Proteins (g/dl)	4.17±0.33	6.20±0.23	4.20±0.23
TC (mg/dl)	67.40±1.08	96.80±4.96	82.40±2.11
TG (mg/dl)	72.80±1.28	90.40±1.75	76.00±2.45
HDL (mg/dl)	23.20±0.86	55.00±3.08	33.40±1.60
LDL (mg/dl)	20.61±1.11	34.00±1.84	21.00±1.14
VLDL (mg/dl)	23.09±1.32	25.40±1.63	32.20±1.59

Abbreviations: AgNP, silver nanoparticle; ALP, alkaline phosphatase; ALT, alanine transferase; AST, aspartate transferase; HDL, high-density lipoprotein; LDL, low-density lipoprotein; MSA, mouse serum albumin; TC, total cholesterol; TG, triglyceride; VLDL, very low-density lipoprotein.

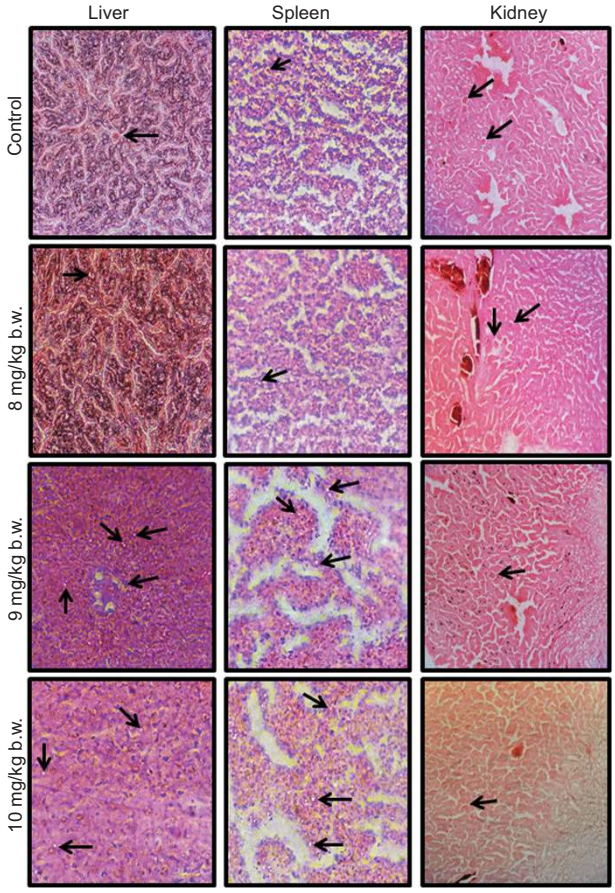

Figure 3 Histopathology of liver, spleen and kidney tissue from mice treated with increasing doses of AgNP-MSA, observed under a light microscope (Nikon TS 100 ECLIPSE). The liver was found to have normal architecture in all treated groups except those exposed to 9 and 10 mg/kg b.w. of AgNP-MSA. Necrotic spots of hepatocytes and hydropic degeneration (black arrows) around the central vein were observed at these dosages. At the 10 mg/kg b.w. dosage, inflammatory cells were found in the sinusoidal spaces, and multifocal lesions were observed in the liver. Due to the increased proliferation of local macrophages, minor lesions were observed in the 10 mg/kg b.w. AgNP-MSA-treated spleen. No abnormality was observed in the kidney. AgNP, silver nanoparticle; MSA, mouse serum albumin.

Effect of AgNP-MSA on the size and appearance of murine fibrosarcoma

After subcutaneous injection of MCA and PMA, the tumor appeared to be hard, round, well confined and palpable with pronounced inflammation, whereas the tumors that appeared in the nanoparticle-treated mice were soft, not well confined and flat (Figure 6a). Histological examination at the fortieth week showed that there was no significant difference in the tumor cell morphology in the AgNP-MSA-treated and non-treated mice (data not shown). However, there was a significant difference in the tumor size. The maximum tumor size found in the AgNP-treated was 2.8±0.62 mm, whereas the average

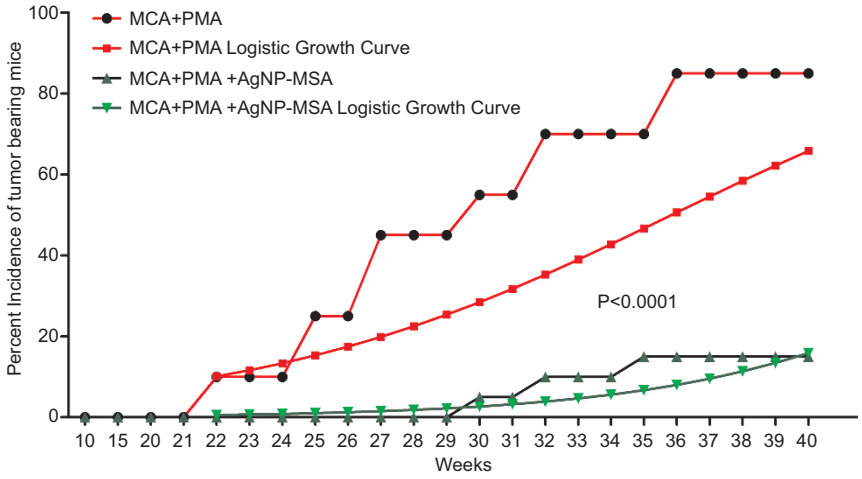

Figure 4 Effect of AgNP-MSA (4 mg/kg b.w./alternate day) on the MCA-induced PMA-promoted tumor incidence in the Swiss albino mice. The percentage of mice with tumors and the logistic growth curve were plotted as a function of the number of weeks of the test ($P<0.0001$). AgNP, silver nanoparticle; MSA, mouse serum albumin; PMA, phorbol myristate 13-acetate.

tumor size in the non-treated group at the fortieth week was 8.1±0.8 mm (Figure 6b, $P<0.0001$).

Transmission electron micrograph analysis of AgNP-MSA-treated tumor tissue

This study showed that there was considerable uptake of AgNP-MSA by immune cells associated with fibrosarcoma tissue. The immune cells containing AgNP-MSA were found to be damaged and also progressed towards cell death; this result was in contrast to non-treated fibrosarcoma tissue. A more muddled plus patchy cellular structure was observed in the AgNP-MSA-treated fibrosarcoma, suggesting that the AgNP-MSA treatment caused pyknotic primary sentinel immune cells to infiltrate the fibrosarcoma tissue (Figure 7).

Effect of AgNP-MSA on the serum TNF-α, IL-6 and IL-1β levels in murine fibrosarcoma

The serum levels of TNF-α, IL-6 and IL-1β were determined every other week from the first injection of MCA. There was an exponential shift in the TNF-α production from the twentieth week after the first injection of MCA in the tumor-induced group compared with the AgNP-treated tumor-induced group. During the first week, 287.55±3.31 pg/ml and 270.55±24.79 pg/ml of TNF-α production was observed in the non-treated and AgNP-treated tumor group, respectively. During the twentieth, twenty-fourth and twenty-sixth weeks, the level of TNF-α in the tumor group was 487.80±7.15 pg/ml, 974.10±17.81 pg/ml and 1134.35±19.6 pg/ml, respectively, while during the fortieth week, the level of TNF-α was 1198.55±99.7 pg/ml. This shift was not observed in the AgNP-treated tumor group; the level during the 20th week was 301.85±12.45 pg/ml, and the level during the twenty-sixth and fortieth weeks was 303.75±18.08 pg/ml, 334.6±14.6 pg/ml, respectively (Figure 8a). From a statistical point of view, the average TNF-α production for the AgNP-treated group was significantly lower than that of the non-treated tumor-bearing group ($P<0.01$).

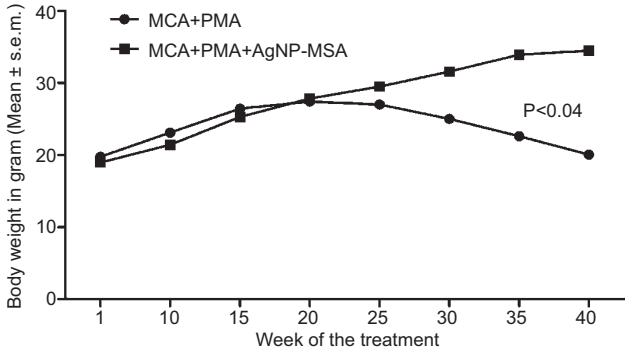

Figure 5 Effect of AgNP-MSA (4 mg/kg b.w./alternate day) on the body weight of mice with chemically induced murine fibrosarcoma. The results are expressed as the mean±standard error mean, and the results were found to be significant at a level of $P<0.04$. AgNP, silver nanoparticle; MSA, mouse serum albumin.

The IL-6 level was 221.70±27.09 pg/ml and 219.55±7.46 pg/ml in the non-treated tumor-bearing and AgNP-MSA-treated tumor-bearing groups, respectively, during the first week of MCA injection. During the twenty-second week, the first significant difference was observed, and there was a shift from 221.70±27.085 pg/ml to 430.950±27.4366 pg/ml of IL-6 production in the non-treated tumor-bearing group. During the fortieth week, this level increased to 730.450±25.01636 pg/ml; in contrast, during the twenty-second and fortieth weeks, the IL-6 production of the AgNP-MSA-treated tumor-bearing group was 259.25±19.25 pg/ml and 339.15±20.5 pg/ml, respectively (Figure 8b) ($P<0.0005$). Thus, the production of this particular cytokine did not shift compared to that in the non-treated tumor-bearing group.

The NBT assay

The standardized colorimetric NBT assay was used to compare the superoxide anion produced in various tissues. Tissue was

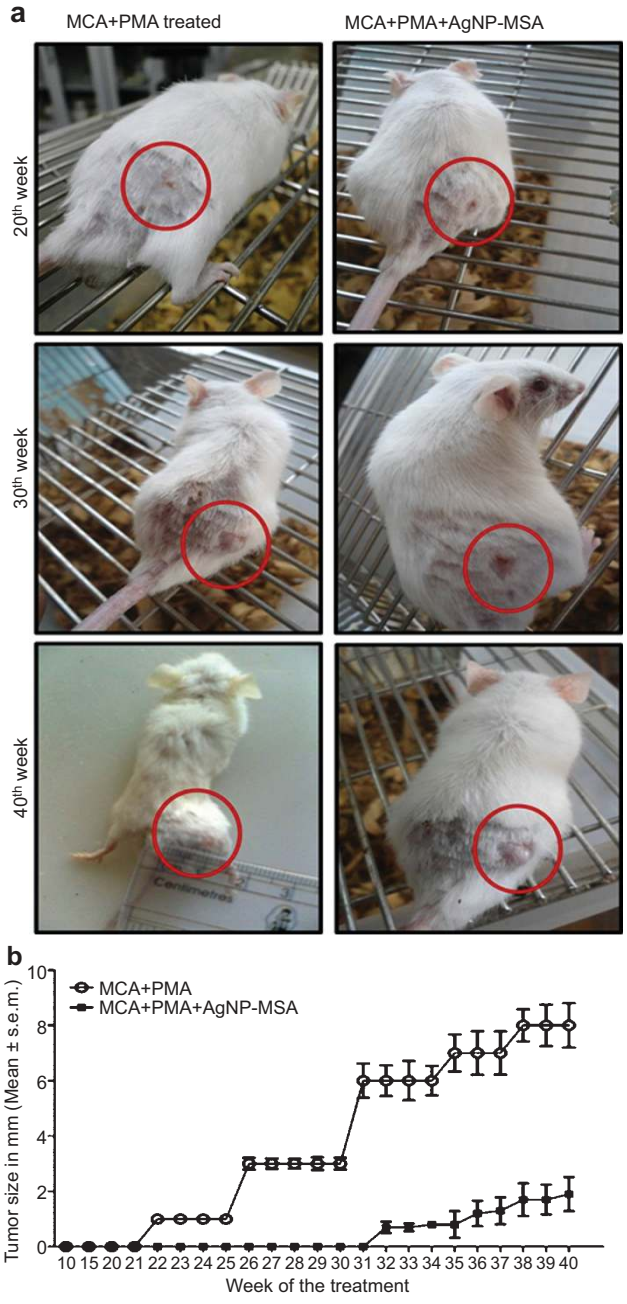

Figure 6 (**a**) Photograph of a tumor induced by the 0.5 mg/dose of MCA and promoted by PMA in the right flank of the Swiss albino mice and also of the tumor group treated with the 4 mg/kg b.w. dosage of AgNP-MSA. Photographs were taken at the twentieth, thirtieth and fortieth weeks of the experiment. (**b**) Effect of AgNP-MSA on the tumor size in chemically induced murine fibrosarcoma; the results are expressed as the mean±s.e.m. ($P<0.0001$). AgNP, silver nanoparticle; MSA, mouse serum albumin; PMA, phorbol myristate 13-acetate; s.e.m., standard error mean.

obtained from the liver, spleen, kidney and tumor of MCA+PMA-treated mice and from MCA+PMA+AgNP-MSA-treated mice. In the liver, spleen and kidney, there was no significant ($P>0.05$) difference between the two groups. However, the tumor tissue showed a significantly lower oxygen content, which was indicative of a hypoxic condition and was restored to normoxic levels after treatment with AgNP-MSA; this treatment resulted in a significant ($P<0.001$) increase in the oxygen content in the tumor tissue (Figure 9a).

Nitric oxide release assay

Nitric oxide release was measured to predict the RNS level and iNOS function in the liver, spleen, kidney and tumor tissue that was obtained from the MCA+PMA-treated and MCA+PMA-treated group and for treatment with AgNP-MSA. The RNS levels were not significantly altered ($P>0.05$) in the liver, spleen and kidney. However, in the tumor tissue, the RNS level was found to be significantly lower than that in other tissues ($P<0.005$) and was found to be restored to normal tissue levels ($P<0.01$) by the AgNP-MSA treatment (Figure 9b).

Immunocytochemistry and serum profile of IL-1β

For IL-1β, there was a dramatic arrest in IL-1β at a significance level of 0.01. Since the initiation time of tumor at the twenty-second week, the release of this pro-inflammatory cytokine significantly increased. In contrast, in the AgNP-MSA-treated group, there was total attest of the IL-1β release, and the IL-1β levels had no significant difference ($P>0.05$) between the first and the fortieth weeks (Figure 10a).

To further determine whether IL-1β was degraded or functionally inhibited (possibly by the formation of a AgNP-IL-1β corona) after the AgNP treatment in the tumor environment, we used immunocytochemistry to analyze the IL-1β in the SCS isolated from both treated and nontreated tumor tissue. In the tumor tissue, the IL-1β expression was high, whereas in the AgNP-MSA-treated tumor tissue, the IL-1β level was low (Figure 10b).

DISCUSSION

The therapeutic application of nanoparticles has gained importance in medicine due to the reduced size and large surface-to-volume ratio of nanoparticles. Recently, accumulated data suggested greater considerations about the use of AgNPs in therapeutics due to their toxicity compared with other noble metal nanoparticles. Our study aimed to analyze the toxicity of AgNPs at different doses in a murine model and to study the application of AgNPs for targeting murine fibrosarcoma. Tiwari *et al.*[19] in 2011 studied the toxicity of AgNPs in the doses of 4 mg, 10 mg, 20 mg and 40 mg/kg b.w. in Wistar rats and concluded that doses near 4 mg/kg body weight were best suited for the therapeutic application.[19] The low dose range of 1–10 mg/kg b.w. has thus been prioritized to avoid the higher doses that would have been obviously toxic. The bioavailability analysis of AgNP and albumin-coated AgNP (AgNP-MSA) showed that the coated particles had enhanced uptake by mice compared to the uncoated particles, and this finding demonstrated that the protein-coated nanoparticles have increased biocompatibility (Table 2). This bioavailability finding was also correlated with other findings, which showed that coating nanoparticles with albumin reduces the chances of interaction with other serum proteins because albumin is the most abun-

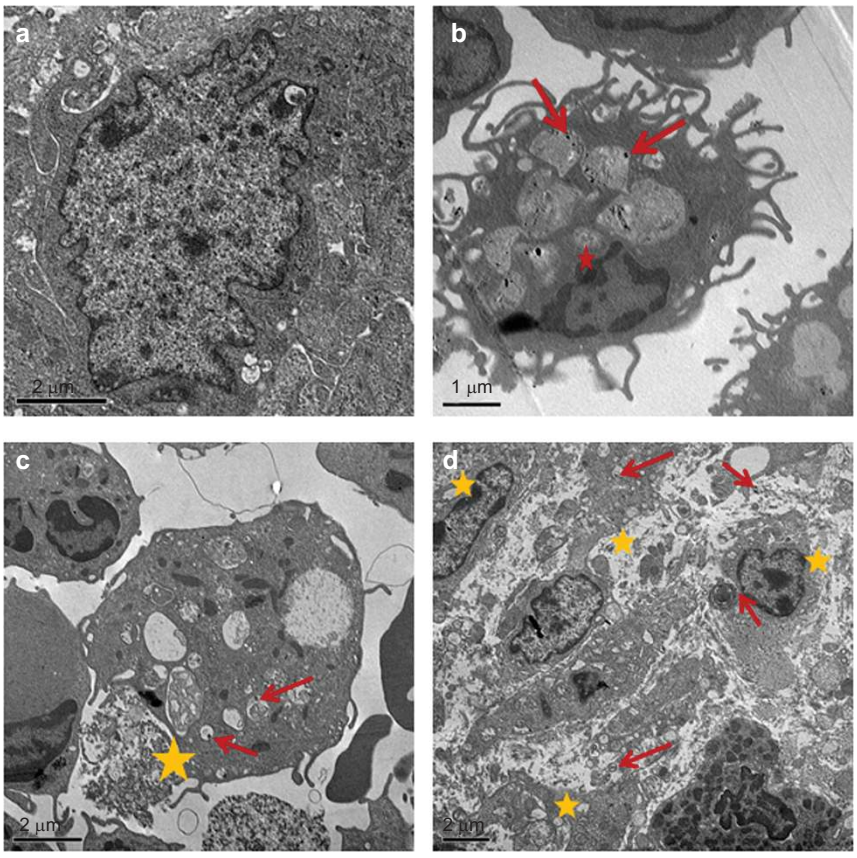

Figure 7 TEM images of fibrosarcoma cells of AgNP-MSA-treated tumor-bearing mice. (**a**) Langerhans cells associated with fibrosarcoma tissue (not treated with nanoparticles) (bar is 2 μm). (**b**) Uptake of AgNP-MSA by dendritic cells associated with fibrosarcoma tissue (red arrows show the nanoparticle presence; red star shows the formation of an initial pyknotic nucleus in this nanoparticle-containing cell) (bar=1 μm). (**c**) Deformed structure of nanoparticle-containing immune cells of fibrosarcoma tissue (the red arrow shows nanoparticle presence, and the yellow star shows the damaged morphology of the nanoparticle-containing immune cells of the fibrosarcoma tissue) (bar=2 μm). (**d**) Overall deformed intracellular structure of nanoparticle-containing immune cells of the fibrosarcoma tissue (the yellow star shows the buckled intracellular morphology of immune cells associated with the fibrosarcoma tissue; the red arrow shows the presence of AgNP-MSA) (bar=0.2 μm). AgNP, silver nanoparticle; MSA, mouse serum albumin; TEM, transmission electron microscopy.

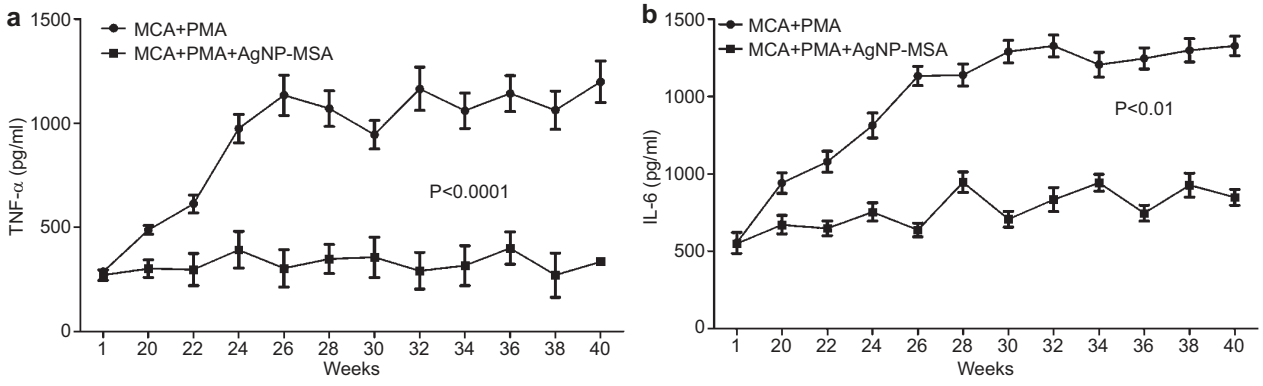

Figure 8 (**a**) Effect of AgNP-MSA (4 mg/kg b.w./alternate day) on the release of TNF-α in the murine fibrosarcoma. The results are expressed as the mean±s.e.m. Serum TNF-α level (pg/ml) plotted as a function of the number of weeks of the experiment ($P<0.01$). (**b**) Effect of AgNP-MSA (4 mg/kg b.w.) on the IL-6 release in the murine fibrosarcoma. The results are expressed as the mean ± s.e.m. Serum IL-6 level (pg/ml) plotted as a function of the number of weeks of the experiment ($P<0.01$). AgNP, silver nanoparticle; MSA, mouse serum albumin; s.e.m., standard error mean.

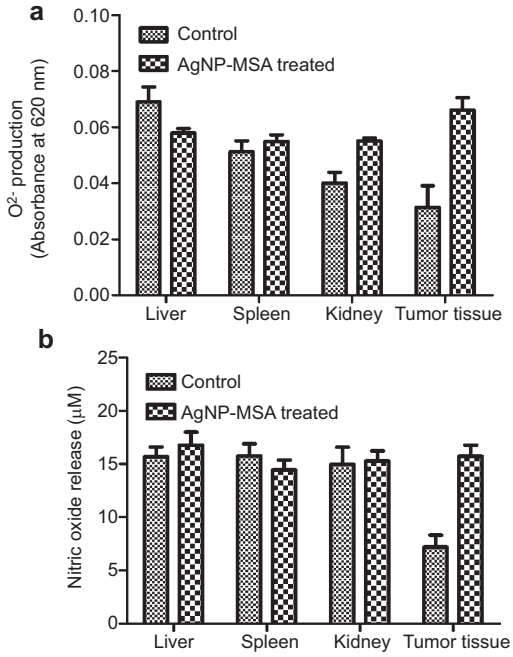

Figure 9 Effect of AgNP-MSA on the O^{2-} and NO generation in the tumor tissue of murine fibrosarcoma. (**a**) Level of the O^{2-} free radical in the SCS isolated from both AgNP-MSA-treated and non-treated tumor tissue ($P<0.001$). (**b**) Level of NO in the SCS isolated from both AgNP-MSA-treated and non-treated tumor tissue ($P<0.005$). The results are expressed as the mean±s.e.m. AgNP, silver nanoparticle; MSA, mouse serum albumin; SCS, single cell suspension; s.e.m., standard error mean.

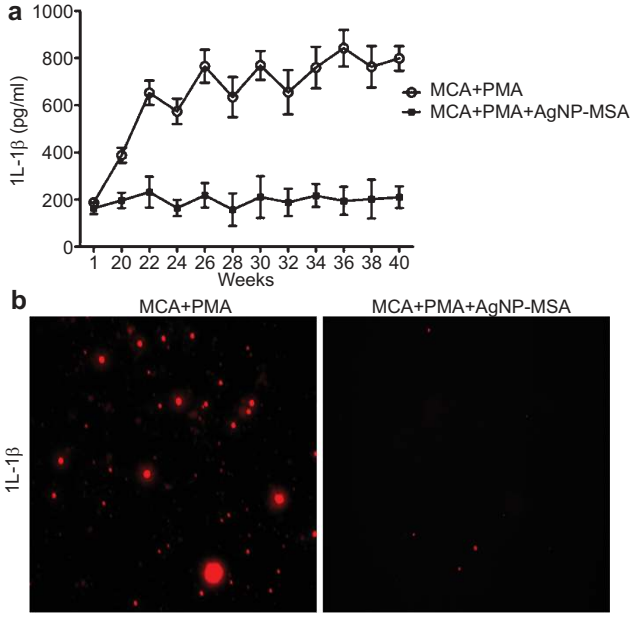

Figure 10 (**a**) Serum level of IL-1β every week during the experimental period in the AgNP-MSA-treated and non-treated murine fibrosarcoma groups. The data are presented as the mean±s.e.m. ($P<0.01$). (**b**) Immunofluorescence picture of IL-1β in the SCS isolated from tumor tissue and from the AgNP-MSA-treated tumor tissue after the fortieth week of the experiment. AgNP, silver nanoparticle; MSA, mouse serum albumin; SCS, single cell suspension; s.e.m., standard error mean.

dant serum protein; thus, this functionalization enhanced the uptake by surrounding cells even at very low doses of nanoparticles.[35,36] Albumin has been used to increase the bioavailability of nanoparticles. Because of the structural homology among various types of albumin, the serum albumin from any other species, such as bovine serum albumin from cows, could have been used. However, to minimize any risk of immunogenicity arising from albumin, MSA was chosen as the preferred form for the protein functionalization of NPs in this study. This selection was an extra precautionary measure that was possibly redundant because BLAST showed a conserved domain in the albumin protein sequences in the tetrapoda family. For other species, species-specific albumin may be used.

Time scale studies were performed to study the systemic toxicity, as measured through the hepatic and renal functions, the blood parameters and the histological parameters in normal mice that received different doses ranging from 1–10 mg/kg b.w. (Supplementary Figure 1 and Supplementary Figure 2).

This toxicological study showed that for doses ranging from 2–8 mg/kg b.w., the WBC, LC and granulocyte counts increased in the non-tumor induced mice, whereas the doses of 9 and 10 mg/kg b.w. showed conclusive toxicity in the non-tumor induced mice. This change was indicated by the elevated levels of ALT and AST, classical markers of liver function, and the serum creatinine level, a marker for renal function.

After the IC50 of AgNP-MSA (6.15 mg/kg b.w.) was measured in mice, the next phase was to analyze the effect in a murine *in vivo* model of fibrosarcoma. The effect of AgNP-MSA was studied by constantly monitoring the tumor incidence, body weight and tumor size of murine fibrosarcoma for 40 weeks. Moreover, the toxicity study showed a relation between AgNP-MSA and immune parameters, which led us to study the effect on the serum levels of TNF-α and IL-6 in murine fibrosarcoma. The toxicity profile of AgNPs in mice at 10 doses was obtained by measuring the complete blood count, lipid profile and histology. This study showed that AgNP doses ranging from 2 to 8 mg/kg b.w. in the control group increased the WBC, LC and granulocyte counts, whereas the other parameters were unchanged. The 9 and 10 mg/kg b.w. doses showed systemic toxicity in control mice. Thus, the results implied that the AgNPs administered *in vivo* (s.c.) were creating an immune response in the non-tumor induced mice.

A possible reason for this finding is that nanoparticles interact with proteins, nucleic acid, and lipids and are often adsorbed by proteins inside biological systems through the formation of a nanoparticle–protein corona (NP–PC), which influences biological activity.[37] This NP–PC formation is aided by several forces, such as hydrogen bonds, solvation forces, van der Waals interaction, and others.[38,39] Nanoparticles can also modify the structure and therefore, the function of the adsorbed proteins in NP–PCs, which thus alter the overall activity of the nanoparticles. This modification of the adsorbed proteins in NP–PCs may involve specific foldings, which may lead to a

change in the conformation of the epitopes of the adsorbed protein.[40] Moreover, nanoparticles can change continuous epitopes of the adsorbed protein, affecting a stretch of 10–12 amino acids, and this stretch is capable of eliciting an immune response. Thus, by forming NP–PCs in biological systems, nanoparticles can induce an abnormal unfolding of adsorbed proteins, which may result in an unwanted immune response through the exposure of hidden epitopes.[40] Hence, the unwanted immune responses induced by AgNPs in our study, as evident from the increase in the WBC, lymphocyte and granulocyte counts, might result from NP–PC formation in mice and the from the subsequent sequential exposure of hidden epitopes of the adsorbed proteins. Additionally, the curved (spherical) surface of nanoparticles compared to planar surfaces provide extra flexibility and enhanced surface area to the adsorbed protein molecule.[39]

In our study, spherical AgNPs were used, and our results showed a significant increase in the WBC, lymphocyte and granulocyte counts even at extremely low doses (2 mg/kg b.w.). This increase might be due to the spherical nature of the AgNPs inside the mice; this shape provided increased flexibility and an enhanced surface area to the adsorbed NP–PC proteins, resulting in an unwanted immune response even at very low doses. Moreover, lymphocytosis, i.e., an increase in the lymphocyte count over the granulocyte count, was observed after AgNP administration. In more detail, in a study on tumor regression in response to chemotherapy, lymphocytosis was reported in patients independent of tumor histotype and chemotherapeutic regimen, with a significantly higher mean lymphocyte count at the end of the chemotherapeutic treatment with respect to the values observed before the onset of treatment.[41] Recent advances in tumor immunobiology suggest that cancer chemotherapy may have the dual functions of cytotoxic activity combined with immunomodulatory effects involving endogenous cytokine action to control both tumor angiogenesis and antitumor immunity. The action of nanomaterials as potent chemotherapeutic agents on lymphocyte-mediated anticancer immunity must still be investigated and elucidated. Chemotherapy itself may paradoxically act, at least in part, as a cancer immunotherapy by inducing lymphocytosis, most likely to modulate the cytokine network and correct the altered endogenous production of the cytokines responsible for cancer-related immunodeficiency.

In relation to the immunomodulatory properties of AgNPs in normal mice observed in our study, we opted for a chemically induced fibrosarcoma for an antitumor study of these nanoparticles. The chemically induced fibrosarcoma is known to have unique antigenic individuality and has been a favorite choice of tumor immunologists.[28] In our study, in the group that was administered MCA, fibrosarcoma appeared during the twenty-second week of the treatment and grew continuously until the thirty-sixth week. The effective accumulation of nanoparticles in tumors, as observed in our ICP–AES data, is a prerequisite for NP-assisted cancer diagnosis and treatment. The ICP–AES analysis clearly showed that unlike AgNP, AgNP-MSA is effectively cleared from the liver, spleen and kidney of mice. In contrast, naked AgNP tended to accumulate in the said tissues and in fibrosarcoma tissue (Table 2) at a significantly very high amount. The lack of effective clearance and the subsequent bio-accumulation after an *in vivo* treatment with NPs is tantamount to systemic toxicity. Hence, further assays of the *in vivo* antitumor effect of AgNPs were redundant and were thus performed with AgNP-MSA alone.

It was hypothesized that the aggregation of NPs stimulated by a tumor microenvironment can be utilized to enhance the retention and cellular uptake of NPs in tumors. AgNPs (approximately 10 nm) showed a fast, sensitive, and reversible response to the pH change from pH 7.4 to pH 6.5, which enabled the AgNPs to be well dispersed at pH 7.4, while quickly aggregating at pH 6.5. The MSA-AgNPs were found to be stable at the pH of blood and normal tissues and thus exhibited an excellent stealth ability to resist uptake by macrophages; however, the MSA-AgNPs aggregated instantly in response to the acidic extracellular pH of solid tumors, leading to greatly enhanced uptake by cancer cells.[42] Moreover, the patterns of blood circulation and the clearance profile of nanomaterials *in vivo* must be understood to ward off unwanted toxicity before these materials can be used in biomedicine.

Nanomaterials have heterogeneous characteristics that combine the bulk properties of solids with quantum phenomena, largely due to their high surface-to-volume ratio, which enables them to exhibit diverse functionalities. Smaller nanomaterials (10–20 nm) are rapidly taken up in the liver from the blood, whereas larger nanomaterials (>200 nm) are efficiently taken up by Kupffer cells in the liver. In the splenic sinusoids, as blood flows through the venous system, nanoparticles larger than 200 nm are cleared by splenic filtration with the help of macrophages. The capillary fenestrae of the glomeruli can allow particles of 10–100 nm size to pass through, but particles with sizes greater than 100 nm are blocked by the basal lamina.[43] Because the particle size in the study was approximately 10 nm, any AgNP that escaped entry into the tumor microenvironment and entered the systemic circulation was effectively cleared from the body.

Tumor promotion or induction is correlated with body weight loss, and this correlation was also observed in our study. Thus, physiological parameters, such as tumor incidence, tumor size and body weight loss, were monitored for 40 weeks in both the AgNP-MSA-treated and non-treated groups. In the AgNP-MSA (4 mg/kg b.w.)-treated mice, the first tumor incidence was delayed by 9 weeks. In addition to this finding, the tumors of the AgNP-MSA-treated mice were significantly ($P<0.0001$) smaller (2.6 mm) than those of the non-treated group (8 mm) after the fortieth week. We found a significant decrease in the body weight in almost 50% of the MCA-induced tumor-bearing mice compared to the normal mice; this change suggests that cancer cachexia has occurred. Moreover, the body weight of the AgNP-MSA-treated mice was also found to be normal. Thus, we suggest that AgNP-MSA not only inhibited the tumor incidence but also helped

to overcome the progressive body weight loss of tumor-bearing mice.

The electron micrographs showed that compared to the non-treated tumor, the AgNP-treated tumor had a more deformed structure of the sentinel immune cells associated with the tumor. The sentinel immune cells associated with the fibrosarcoma (e.g., Langerhans cells/dendritic cells and others) take up AgNP-MSA considerably more readily than other cells; therefore, the dendritic cells in our study showed substantial uptake of AgNP-MSA (Figure 7). The result from this micrograph suggested an effect of AgNP on immune cells that was also analogous with the unwanted immune response observed in normal mice. The immune cells associated with any tumor are known to be involved in cancer progression through inflammatory mediators, and the AgNP antitumor effect indicated by previous parameters of our study might be caused by the cytotoxic effect on immune cells by the same mechanism as suggested from the electron micrographs.

This study reports an immune response to AgNP-MSA in normal mice, reductions in tumor incidence and tumor size, and a countering of the loss of body weight in MCA-treated mice; thus, the next relevant question is whether there was any immune modulation by the AgNP-MSA in the fibrosarcoma tumor microenvironment. To address this possibility, the serum levels of two important cytokines, TNF-α and IL-6, were measured during the experimental period. These two cytokines are known to be associated with cancer cachexia[44,45] and also play an important role in tumor progression.[46,47] The serum levels of both these cytokines were found to be positively related with tumor promotion. The AgNP-treated tumor group showed normal cytokine levels, which were consistent with other physiological parameters. The tumor microenvironment has distinctive proteins or cellular environments, and NPs that are exposed to several, very different systems *in vivo* can form bio/nanocomplexes, which ultimately determine the activity of nanoparticles inside a particular system. Thus, this result most likely explains the possibility that AgNP-MSA in the fibrosarcoma microenvironment downregulated the proinflammatory cytokine levels.

In more detail, it has been reported that pelted nanoparticles in an *in vivo* system may pass through the peritoneal and mucosal layers of gut epithelial cells and finally, enter the bloodstream. At cellular levels, the NPs that have been phagocytosed by a monocyte may be taken into the endosomes that ultimately fuse with lysosomes.[48] Each of these proteomes represents a unique environment and has specific properties in terms of protein composition, enzymatic activities, pH, ion composition and other characteristics; these properties determine the fate of the nanoparticles. Thus, in our study, the subcutaneous administration of AgNP-MSA in the murine fibrosarcoma might lead to the formation of a unique bionanocomplex compared to that in control mice, and this change ultimately downregulated these two cytokine levels.

The amount of proteins available to interact with the nanoparticle surface can also greatly influence the NP–PC composition.[49] In an *in vivo* system, as a nanoparticle passes through different protein-rich environments, the nanoparticle surface may become pre-coated with specific proteins that affect the possible binding to the next protein to form more nanoparticle–protein complexes.[50] The affinity of the protein for the NP surface also determines whether the protein can completely occupy the surface or not. The sequential arrangement of protein molecules bound to the nanoparticle surface may affect the biological reactivity.[51] Thus, the different cellular organizations or protein-rich tumor microenvironments in our results might explain the fact that AgNP-MSA forms different NP–PC corona, which, consequently, counteract the protumorigenic immune regulation by inhibiting the release of these cytokines. Moreover, in the tumor immune microenvironment, there are multiple immune checkpoints that control the tumor surveillance inside organisms.[52] The cytokine levels in the different experimental groups showed a tumor immunomodulation by the AgNP-MSA, which ultimately affects the immune checkpoints.

The ICP–AES data and electron micrograph showed that at a dose of 4 mg/kg b.w., the AgNP-MSAs were significantly present in tumor fibrosarcoma due to direct pelting of the nanoparticles in the flank containing the fibrosarcoma. This result may also be caused by the immune cells associated with the tumor microenvironment predominantly taking up the AgNPs because of the decreased possibility of nonspecific NP–PC formation by AgNP-MSA. Consequently, the anticancer property found in our study must be executed through immune cells. To obtain more insight into this role, we performed experiments studying the oxidative status of the tumor microenvironment of both AgNP-MSA-treated and untreated groups. Oxidative parameters were mainly selected because nanoparticles are known to be associated with the oxidative stress response in many cells or tissue.[53] We measured the NBT (O_2^- radical measurement) and nitric oxide (NO) of the SCS isolated from both AgNP-MSA-treated and non-treated fibrosarcoma. The results showed that these nanoparticles significantly increased these two parameters in the SCS isolated from fibrosarcoma (Figure 9), and the anticancer property demonstrated by AgNP can be attributed to this increase in oxidative stress in the tumor microenvironment.

One of the prime facts of tumor promotion and surveillance is that immune cells (especially macrophages) associated with the tumor microenvironment mainly promote the tumor.[54] Thus, the AgNP-containing immune cells or other cells mainly encounter oxidative stress, which might have collectively contributed to the anticancer response. The result was further supported by recent *in vitro* findings, where it has been reported that AgNPs can induce the apoptosis of RAW through an increase in oxidative stress.[55,56] Moreover, the downregulation of the protumorigenic cytokines TNF-α and IL-6 in the AgNP-treated fibrosarcoma group also demonstrated that AgNP significantly altered the cell function of tumor-associated immune cells. Furthermore, the hypoxic condition (low oxygen condition) of a solid tumor is known to be associated

with tumor promotion, and in our study, AgNPs significantly increased the oxygen free radical and NO levels in the tumor microenvironment, which oppose hypoxia. Additionally, because of the inflammatory condition provided by the MCA-induced fibrosarcoma, many proinflammatory molecules play a role in tumor promotion.

Among the target proteins that are likely to be involved in NP–PC formation (discussed earlier), one signature candidate is the pro-inflammatory cytokine IL-1β.[57] IL-1 signaling is the major alarm mechanism that persists in a tumor microenvironment, and IL-1 is produced by cells in a malignant or micro environment. This signaling has contrasting roles, such as the control and promotion of tumors, and these roles are mediated by two important agonists called IL-1α and IL-1β, respectively.[58] The membrane-associated IL-1α has antitumor properties and is generally expressed at a very low level in tumor microenvironments, whereas IL-1β has a role in the promotion of carcinogenesis, tumor invasiveness, and immunosuppression. IL-1β is expressed as a secretory molecule in large quantity in tumor microenvironments.[58] In addition, particularly in the MCA-induced tumor immune microenvironment, this IL-1β-mediated tumor progression mostly persists.[59] Interestingly, AgNPs were also reported to have inhibitory effects on the cell signaling mediated by IL-1β.[60]

Considering these above facts, one possibility behind the functional modulation of the fibrosarcoma immune microenvironment by AgNPs is that AgNPs might have formed coronas with IL-1β (say, AgNP-IL-1β), thus disrupting the IL-1β mechanism of action either through degradation or through functional inhibition. To confirm this possibility, we performed immunocytochemistry analysis of IL-1β in both AgNP-treated and non-treated fibrosarcoma. The result from this experiment showed that there was a nearly negligible amount of IL-1β in the AgNP-treated fibrosarcoma compared to the non-treated fibrosarcoma (Figure 10). Thus, this finding strongly suggested that AgNPs not only modulate the tumor-associated cell function through oxidative stress but also alter the IL-1β function to facilitate the anticancer property against murine fibrosarcoma. Hence, our study showed a direct relationship between AgNP-MSA and immune regulation, as demonstrated by the unwanted response in normal mice and the inflammatory regulation in the murine fibrosarcoma.

CONCLUSION

This study reports a relation between AgNP-MSA and the immune system in a murine model. The study also established the fact that AgNP-MSA showed an unwanted immune response in control mice even at very lower doses, whereas AgNP-MSA showed a rather beneficial immunomodulation that inhibited murine fibrosarcoma by altering the immune microenvironment. In our next article, we will be focusing on the detailed mechanism by which AgNPs lead to the oxidative stress-induced immunomodulation of tumor-associated macrophages.

AUTHORS' CONTRIBUTIONS

All the authors contributed significantly to this research work.

ACKNOWLEDGEMENTS

We gratefully acknowledge the following organizations and institutes for supporting the work.

1. Department of Biotechnology, Govt. of India for providing the DBT Research Associate fellowship to Dr Biswajit Chakraborty.
2. University Grant Commission, Government of India for providing a doctoral research fellowship to Ramkrishna Pal, Leichombam Mohindro Singh and Dewan Shahidur Rahman.
3. Sophisticated Analytical Instrument Facility, Indian Institute of Technology, Mumbai, India for analyzing the inductively coupled plasmon-atomic emission spectra.
4. Sophisticated Analytical Instrument Facility, North Eastern Hill University, Shillong, Meghalaya, India for TEM analysis.
5. Pasteur Institute, Shillong, Meghalaya, India for providing experimental animals.

Supplementary Information accompanies the paper on *Cellular & Molecular Immunology*'s website. (http://www.nature.com/cmi).

1 Keenan BP, Jaffee EM, Armstrong TD. Tumor immunology: multidisciplinary science driving basic and clinical advances. *Cancer Immunol Res* 2013; **1**: 16–23.
2 Zolnik BS, Gonzalez-Fernandez A, Sadrieh N, Dobrovolskaia MA. Nanoparticles and the immune system. *Endocrinology* 2010; **151**: 458–465.
3 Edwards-Jones V. The benefits of silver in hygiene, personal care and healthcare. *Lett Appl Microbiol* 2009; **49**: 147–152.
4 Chen X, Schluesener HJ. Nanosilver: a nanoproduct in medical application. *Toxicol Lett* 2008; **176**: 1–12.
5 Mukherjee S, Chowdhury D, Kotcherlakota R, Patra S, Vinothkumar B, Bhadra MP *et al*. Potential theranostics application of bio-synthesized silver nanoparticles (4-in-1 system). *Theranostics* 2014; **4**: 316–335.
6 Jain J, Arora S, Rajwade JM, Omray P, Khandelwal S, Paknikar KM *et al*. Silver nanoparticles in therapeutics: development of an antimicrobial gel formulation for topical use. *Mol Pharm* 2009; **6**: 1388–1401.
7 Lee HY, Park HK, Lee YM, Kim K, Park SB. A practical procedure for producing silver nanocoated fabric and its antibacterial evaluation for biomedical applications. *Chem Commun (Camb)* 2007; **28**: 2959–2961.
8 Vigneshwaran N, Kathe AA, Varadarajan PV, Nachane RP, Balasubramanya RH. Functional finishing of cotton fabrics using silver nanoparticles. *J Nanosci Nanotechnol* 2007; **7**: 1893–1897.
9 Kokura S, Handa O, Takagi T, Ishikawa T, Naito Y, Yoshikawa T. Silver nanoparticles as a safe preservative for use in cosmetics. *Nanomed Nanotechnol Biol Med* 2010; **6**: 570–574.
10 Haase H, Fahmi A, Mahltig B. Impact of silver nanoparticles and silver ions on innate immune cells. *J Biomed Nanotechnol* 2014; **10**: 1146–1156.
11 Bhol KC, Schechter PJ. Topical nanocrystalline silver cream suppresses inflammatory cytokines and induces apoptosis of inflammatory cells in a murine model of allergic contact dermatitis. *Br J Dermatol* 2005; **152**: 1235–1242.
12 Gagne F, Auclair J, Fortier M, Bruneau A, Fournier M, Turcotte P *et al*. Bioavailability and immunotoxicity of silver nanoparticles to the freshwater mussel *Elliptio complanata*. *J Toxicol Environ Health A* 2013; **76**: 767–777.
13 Myrzakhanova M, Gambardella C, Falugi C, Gatti AM, Tagliafierro G, Ramoino P *et al*. Effects of nanosilver exposure on cholinesterase activities, CD41, and CDF/LIF-like expression in zebrafish (*Danio rerio*) larvae. *BioMed Res Int* 2013; **2013**: 12.

14 Su CL, Chen TT, Chang CC, Chuang KJ, Wu CK, Liu WT *et al*. Comparative proteomics of inhaled silver nanoparticles in healthy and allergen provoked mice. *Int J Nanomed* 2013; **8**: 2783–2799.
15 de Jong WH, van der Ven LT, Sleijffers A, Park MV, Jansen EH, van Loveren H *et al*. Systemic and immunotoxicity of silver nanoparticles in an intravenous 28 days repeated dose toxicity study in rats. *Biomaterials* 2013; **34**: 8333–8343.
16 Liu H, Yang D, Yang H, Zhang H, Zhang W, Fang Y *et al*. Comparative study of respiratory tract immune toxicity induced by three sterilisation nanoparticles: silver, zinc oxide and titanium dioxide. *J Hazard Mater* 2013; **248–249**: 478–486.
17 Greulich C, Kittler S, Epple M, Muhr G, Koller M. Studies on the biocompatibility and the interaction of silver nanoparticles with human mesenchymal stem cells (hMSCs). *Langenbecks Arch Surg* 2009; **394**: 495–502.
18 Lim DH, Jang J, Kim S, Kang T, Lee K, Choi IH. The effects of sub-lethal concentrations of silver nanoparticles on inflammatory and stress genes in human macrophages using cDNA microarray analysis. *Biomaterials* 2012; **33**: 4690–4699.
19 Tiwari DK, Jin T, Behari J. Dose-dependent in-vivo toxicity assessment of silver nanoparticle in Wistar rats. *Toxicol Mech Methods* 2011; **21**: 13–24.
20 Sriram MI, Kanth SB, Kalishwaralal K, Gurunathan S. Antitumor activity of silver nanoparticles in Dalton's lymphoma ascites tumor model. *Int J Nanomedicine* 2010; **5**: 753–762.
21 Maneewattanapinyo P, Banlunara W, Thammacharoen C, Ekgasit S, Kaewamatawong T. An evaluation of acute toxicity of colloidal silver nanoparticles. *J Vet Med Sci* 2011; **73**: 1417–1423.
22 Kim YS, Song MY, Park JD, Song KS, Ryu HR, Chung YH *et al*. Subchronic oral toxicity of silver nanoparticles. *Part Fibre Toxicol* 2010; **7**: 20.
23 Park EJ, Bae E, Yi J, Kim Y, Choi K, Lee SH *et al*. Repeated-dose toxicity and inflammatory responses in mice by oral administration of silver nanoparticles. *Environ Toxicol Pharmacol* 2010; **30**: 162–168.
24 Xue Y, Zhang S, Huang Y, Zhang T, Liu X, Hu Y *et al*. Acute toxic effects and gender-related biokinetics of silver nanoparticles following an intravenous injection in mice. *J Appl Toxicol* 2012; **32**: 890–899.
25 Zhang T, Wang L, Chen Q, Chen C. Cytotoxic potential of silver nanoparticles. *Yonsei Med J* 2014; **55**: 283–291.
26 Gross L. Intradermal immunization of C3H mice against a sarcoma that originated in an animal of the same line. *Cancer Res* 1943; **3**: 326–333.
27 Foley EJ. Antigenic properties of methylcholanthrene-induced tumors in mice of the strain of origin. *Cancer Res* 1953; **13**: 835–837.
28 Noguchi Y, Jungbluth A, Richards EC, Old LJ. Effect of interleukin 12 on tumor induction by 3-methylcholanthrene. *Proc Natl Acad Sci USA* 1996; **93**: 11798–11801.
29 Devens BH, Lundak RL, Byus CV. Induction of murine fibrosarcomas by low dose treatment with 3-methylcholanthrene followed by promotion with 12-O-tetradecanoyl-phorbol-13-acetate. *Cancer Lett* 1984; **21**: 317–324.
30 Lee PC, Meisel D. Adsorption and surface-enhanced Raman of dyes on silver and gold sols. *J Phys Chem* 1982; **86**: 3391–3395.
31 Papadimitriou S, Bikiaris D, Avgoustakis K, Karavas E, Georgarakis M. Chitosan nanoparticles loaded with dorzolamide and pramipexole. *Carbohydrate Polym* 2008; **73**: 44–54.
32 Cavalieri EL, Rogan EG, Higginbotham S, Cremonesi P, Salmasi S. Tumor-initiating activity in mouse skin and carcinogenicity in rat mammary gland of dibenzo[a]pyrenes: the very potent environmental carcinogen dibenzo[a, l]pyrene. *J Cancer Res Clin Oncol* 1989; **115**: 67–72.
33 Choi HS, Kim JW, Cha YN, Kim C. A quantitative nitroblue tetrazolium assay for determining intracellular superoxide anion production in phagocytic cells. *J Immunoassay Immunochem* 2006; **27**: 31–44.
34 Sengupta M, Sharma GD, Chakraborty B. Effect of aqueous extract of *Tinospora cordifolia* on functions of peritoneal macrophages isolated from CCl4 intoxicated male albino mice. *BMC Complement Altern Med* 2011; **11**: 102.
35 Chithrani BD, Chan WC. Elucidating the mechanism of cellular uptake and removal of protein-coated gold nanoparticles of different sizes and shapes. *Nano Lett* 2007; **7**: 1542–1550.
36 Kummitha CM, Malamas AS, Lu ZR. Albumin pre-coating enhances intracellular siRNA delivery of multifunctional amphiphile/siRNA nanoparticles. *Int J Nanomed* 2012; **7**: 5205–5214.
37 Cedervall T, Lynch I, Foy M, Berggård T, Donnelly SC, Cagney G *et al*. Detailed identification of plasma proteins adsorbed on copolymer nanoparticles. *Angew Chem Int Ed Engl* 2007; **46**: 5754–5756.
38 Lundqvist M, Sethson I, Jonsson BH. Protein adsorption onto silica nanoparticles: conformational changes depend on the particles' curvature and the protein stability. *Langmuir* 2004; **20**: 10639–10647.
39 Saptarshi S, Duschl A, Lopata A. Interaction of nanoparticles with proteins: relation to bio-reactivity of the nanoparticle. *J Nanobiotechnol* 2013; **11**: 26.
40 Lundqvist M, Stigler J, Cedervall T, Berggård T, Flanagan MB, Lynch I *et al*. The evolution of the protein corona around nanoparticles: a test study. *ACS Nano* 2011; **5**: 7503–7509.
41 Lissoni P, Fumagalli L, Brivio F, Rovelli F, Messina G, Di Fede G *et al*. Cancer chemotherapy-induced lymphocytosis: a revolutionary discovery in the medical oncology. *J Biol Regul Homeost Agents* 2006; **20**: 29–35.
42 Liu X, Chen Y, Li H, Huang N, Jin Q, Ren K *et al*. Enhanced retention and cellular uptake of nanoparticles in tumors by controlling their aggregation behavior. *ACS Nano* 2013; **7**: 6244–6257.
43 Wang B, He X, Zhang Z, Zhao Y, Feng W. Metabolism of nanomaterials *in vivo*: blood circulation and organ clearance. *Accounts Chem Res* 2012; **46**: 761–769.
44 Figueras M, Busquets S, Carbó N, Almendro V, Argilés JM, López-Soriano FJ. Cancer cachexia results in an increase in TNF-alpha receptor gene expression in both skeletal muscle and adipose tissue. *Int J Oncol* 2005; **27**: 855–860.
45 Barton BE. IL-6-like cytokines and cancer cachexia: consequences of chronic inflammation. *Immunol Res* 2001; **23**: 41–58.
46 Ara T, Declerck YA. Interleukin-6 in bone metastasis and cancer progression. *Eur J Cancer* 2010; **46**: 1223–1231.
47 Balkwill F. TNF-alpha in promotion and progression of cancer. *Cancer Metastasis Rev* 2006; **25**: 409–416.
48 Casals E, Pfaller T, Duschl A, Oostingh GJ, Puntes V. Time evolution of the nanoparticle protein corona. *ACS Nano* 2010; **4**: 3623–3632.
49 Monopoli MP, Walczyk D, Campbell A, Elia G, Lynch I, Bombelli FB *et al*. Physical–chemical aspects of protein corona: relevance to *in vitro* and *in vivo* biological impacts of nanoparticles. *J Am Chem Soc* 2011; **133**: 2525–2534.
50 Gasser M, Rothen-Rutishauser B, Krug HF, Gehr P, Nelle M, Yan B *et al*. The adsorption of biomolecules to multi-walled carbon nanotubes is influenced by both pulmonary surfactant lipids and surface chemistry. *J Nanobiotechnology* 2010; **8**: 31.
51 Ge C, Du J, Zhao L, Wang L, Liu Y, Li D *et al*. Binding of blood proteins to carbon nanotubes reduces cytotoxicity. *Proc Natl Acad Sci USA* 2011; **108**: 16968–16973.
52 Shiao SL, Ganesan AP, Rugo HS, Coussens LM. Immune microenvironments in solid tumors: new targets for therapy. *Genes Dev* 2011; **25**: 2559–2572.
53 Manke A, Wang L, Rojanasakul Y. Mechanisms of nanoparticle-induced oxidative stress and toxicity. *BioMed Res Int* 2013; **2013**: 15.
54 Coussens LM, Werb Z. Inflammation and cancer. *Nature* 2002; **420**: 860–867.
55 AshaRani PV, Low Kah Mun G, Hande MP, Valiyaveettil S. Cytotoxicity and genotoxicity of silver nanoparticles in human cells. *ACS Nano* 2008; **3**: 279–290.

56 Park EJ, Yi J, Kim Y, Choi K, Park K. Silver nanoparticles induce cytotoxicity by a Trojan-horse type mechanism. *Toxicol In Vitro* 2010; **24**: 872–878.
57 Sumbayev VV, Yasinska IM, Garcia CP, Gilliland D, Lall GS, Gibbs BF *et al*. Gold nanoparticles downregulate interleukin-1beta-induced pro-inflammatory responses. *Small* 2013; **9**: 472–477.
58 Voronov E, Dotan S, Krelin Y, Song X, Elkabets M, Carmi Y *et al*. Unique versus redundant functions of IL-1alpha and IL-1beta in the tumor microenvironment. *Front Immunol* 2013; **4**: 177.
59 Krelin Y, Voronov E, Dotan S, Elkabets M, Reich E, Fogel M *et al*. Interleukin-1beta-driven inflammation promotes the development and invasiveness of chemical carcinogen-induced tumors. *Cancer Res* 2007; **67**: 1062–1071.
60 Sheikpranbabu S, Kalishwaralal K, Venkataraman D, Eom SH, Park J, Gurunathan S. Silver nanoparticles inhibit VEGF- and IL-1beta-induced vascular permeability via Src dependent pathway in porcine retinal endothelial cells. *J Nanobiotechnol* 2009; **7**: 8.